Obrabotka metallov (tekhnologiya, oborudovanie, instrumenty) = Metal Working and Material Science. 2026 vol. 28 no. 3 pp. 6–28
ISSN: 1994-6309 (print) / 2541-819X (online)
DOI: 10.17212/1994-6309-2026-28.3-6-28

NSTU NETI

Obrabotka metallov - Metal Working and Material Science

Journal homepage: http://journals.nstu.ru/obrabotka_metallov

Effect of filler morphology on cryogenic treatment sintered PTFE nanocomposites

Vinod Damdhar [1, 2, a, *], *Kavita Pande* [3, b], *Arun Autee* [1, c]

[1] Mechanical Engineering Department, Maharashtra Institute of Technology, Chhatrapati Sambhajinagar (Aurangabad), M.S., 431010, India
[2] Center for Engineering Exploration, C.S.M.S.S. Chh. Shahu College of Engineering, Chhatrapati Sambhajinagar (Aurangabad), M.S., 431010, India
[3] Matverse Vision Pvt Ltd, Nagpur, M.S., 440001, India

[a] https://orcid.org/0000-0002-3719-0157, vinod.damdhar@gmail.com; [b] https://orcid.org/0000-0003-3201-4418, kavita19pande@gmail.com;
[c] https://orcid.org/0000-0003-2132-0532, arun.autee@mit.asia

ARTICLE INFO

Article history:
Received: 02 May 2026
Revised: 25 May 2026
Accepted: 05 June 2026
Available online: 15 September 2026

Keywords:
Sintered *PTFE* composites
Nano-alumina
Nano-mica
Cryogenic treatment
Filler geometry

ABSTRACT

Introduction. Polytetrafluoroethylene (*PTFE*) has outstanding chemical resistance and a low friction coefficient but weak mechanical properties and wear resistance, which restrict its wider use in tribological applications. Thus, ***the present study aims*** to investigate the coupled influence of nano-filler geometry and cryogenic treatment on the structure–property evolution of *PTFE* nanocomposites. **Materials and methods.** The optimized nanocomposite systems (1.0 wt.% nano-mica and 1.5 wt.% nano-alumina), along with neat *PTFE*, were produced by cold compression moulding and sintering. The specimens were soaked for 8, 12, and 16 h in liquid nitrogen at −185 °C and then evaluated for mechanical, tribological, and structural properties using *XRD*, *FTIR*, and *SEM*. **Results and discussion.** Compared to untreated *PTFE* (~27.6 MPa tensile strength), both nano-fillers enhanced the strength and wear resistance. The composites exhibited a strong geometry-dependent response to cryogenic treatment. The tensile strength of mica-filled *PTFE* was at a maximum at 8 h (~37.9 MPa), while alumina-filled *PTFE* reached its peak at 16 h (~36.5 MPa). The same trend was observed for hardness and wear resistance. *XRD* revealed reordering of crystallinity and improved filler–matrix interaction, while *SEM* showed more stable interfaces in the alumina composites. Extended treatment caused interfacial heterogeneity and defects in mica-filled *PTFE*, attributed to its flaky morphology. ***Conclusion.*** Filler geometry is a major determinant of the effectiveness of cryogenic treatment in *PTFE* nanocomposites. Globular nano-alumina exhibited superior tensile strength, hardness, and wear resistance compared to flaky nano-mica after long-term cryogenic treatment. This study presents important structure–property relationships for the development of *PTFE*-based nanocomposites for advanced tribological applications.

For citation: Damdhar V., Pande K., Autee A. Effect of filler morphology on cryogenic treatment sintered PTFE nanocomposites. *Obrabotka metallov (tekhnologiya, oborudovanie, instrumenty) = Metal Working and Material Science*, 2026, vol. 28, no. 3, pp. 6–28. DOI: 10.17212/1994-6309-2026-28.3-6-28. (In Russian).

Introduction

Polytetrafluoroethylene (*PTFE*) is extensively used as a solid lubricant and functional coating owing to its o*UTS*tanding chemical inertness, low coefficient of friction, and high thermal stability over a wide temperature range [1–3]. These features make *PTFE* a popular choice for seals, bearings, gears, piston rings, and non-stick cookware, where low friction and chemical resistance are critical [3, 4, 5–14]. Nevertheless, the inherent low wear resistance and limited load-bearing capacity of neat *PTFE* significantly restrict its application in highly loaded or abrasive environments. Consequently, research has focused on *PTFE*-based micro- and nanocomposites filled with mineral and ceramic particles to achieve substantial improvements in wear resistance without compromising the low-friction behavior [11–15].

*** Corresponding author**
Damdhar Vinod, ME. (Manufacturing Engineering), Assistant Professor
C.S.M.S.S. Chh. Shahu College of Engineering,
Chhatrapati Sambhajinagar (Aurangabad),
431010, M.S., India
Tel.: 91 9607200527, **e-mail:** vinod.damdhar@gmail.com

Nano-mica and nano-alumina are two technologically important yet fundamentally different mineral nano-fillers among the range of reinforcements explored. Nano-mica is a layered silicate with flake-like morphology and a high aspect ratio, which has been found to significantly improve the stiffness, strength, and thermal stability of various polymer matrices, including epoxy, *PS*, *PMMA*, *PAEK*, and *PE*. Conversely, nano-alumina, typically used in equiaxed or near-spherical form, is a hard ceramic that primarily enhances hardness and wear resistance and has become one of the most effective fillers for reducing *PTFE* wear [5–10]. Systematic investigations of *PTFE*/alumina nanocomposites have demonstrated not only a reduction in wear rate by several orders of magnitude at low nano-filler loadings but also the activation of strengthening mechanisms such as particle–fibril interlocking, wear debris refinement, and the formation of stable transfer films [11–15].

Filler geometry and aspect ratio exert a dominant influence on composite behavior, governing particle packing, stress distribution, and crack propagation paths. Plate-like fillers (high aspect ratio), such as mica, provide high-strength anisotropic reinforcement and more efficient load distribution. However, their extended planar interfaces can serve as sites for delamination and crack initiation [8–10]. Studies have shown that mica- and wollastonite-filled *HDPE* exhibit markedly different mechanical properties solely due to particle shape [10], and that platelet alignment and interfacial morphology correlate with variations in friction surface and wear mechanisms in *PTFE*–mica composites [16–18]. In contrast, near-spherical alumina nanoparticles act as more isotropic stress concentrators, promoting three-dimensional load transfer and crack deflection without creating extended weak planes [11–15]. Consequently, even at comparable volume fractions, flake-like nano-mica and globular nano-alumina are expected to generate fundamentally different microstructures and damage evolution patterns in sintered *PTFE*.

In our previous work, we compared nano-mica- and nano-alumina-filled *PTFE* nanocomposites under abrasive pin-on-disc tests at room temperature for filler contents ranging from 0.5 to 5 wt.% [16]. Nano-mica provided an immediate reduction in specific wear rate (*SWR*) reaching a plateau beyond 1 wt.%, making 1 wt.% nano-mica an efficient loading (~16% improvement vs. neat *PTFE*), whereas nano-alumina showed a sharper, content-sensitive response with an optimum at 1.5 wt.% (~22% lower *SWR*), above which agglomeration and third-body abrasion led to performance deterioration [19–29]. That study established optimal nano-filler contents and composition–wear relationships, but did not address the roles of filler geometry or the effect of subsequent cryogenic treatment on the structure–property–wear correlations.

Beyond composition and geometry, cryogenic treatment has emerged as an additional process variable capable of modifying the microstructure and tribological performance of polymeric materials. Deep cryogenic treatment can promote stress relief, alter crystallinity**,** and refine microstructural features, leading to improved wear resistance and dimensional stability in selected systems [17, 26–28]. For *PTFE*-based composites, cryogenic treatment has been investigated for *PTFE*–mica composite coatings for cookware**,** and it was shown that cryo-cycling changes the dominant wear mechanisms and can enhance performance when applied with suitable parameters [16]. Nanoparticle-filled *PTFE* systems have also demonstrated sensitivity of viscoelastic and wear behavior to thermal histories, suggesting that post-processing treatments, including cryogenic exposure, may be used to stabilize microstructures and improve tribological performance [13, 25–30]. However, most existing studies focus either on a single filler type or on coatings rather than bulk sintered components, and systematic comparisons of different filler geometries under cryo-treatment are lacking.

In recent years, the tribological and mechanical properties of *PTFE* composites have been enhanced by the addition of nanoparticles, synergistic hard fillers**,** and cryogenic processing [4, 6, 11–15, 25–30]. However, most available studies are limited either to a single filler system**,** untreated composites, or conventional tribological analysis. Studies on the interaction between filler geometry and cryogenic treatment duration in the structure–property relationships of sintered *PTFE* nanocomposites are still scarce. In particular, there is a lack of comparative data on flake-like nano-mica and globular nano-alumina after extended cryogenic exposure.

The purpose of the present study is to investigate the mechanical, tribological, structural, and microstructural behavior of sintered *PTFE* nanocomposites filled with nano-mica and nano-alumina of different morphologies.

The specific objectives are:

– to fabricate sintered *PTFE*-based nanocomposites with optimized filler contents (1.0 wt.% nano-mica and 1.5 wt.% nano-alumina) together with neat *PTFE* using cold compression moulding and sintering.

– to investigate the effect of cryogenic soaking time (8, 12**,** and 16 h) on the mechanical (tensile strength, compressive strength, hardness, and elongation) and tribological (specific wear rate) properties.

– to determine how flake-like nano-mica and globular nano-alumina affect the filler–matrix interaction, crystallinity, interfacial stability **,** and wear mechanisms under cryogenic treatment.

– to establish correlations between mechanical and tribological behavior and microstructural changes observed by *XRD*, *FTIR***,** and *SEM*.

– to determine the optimum filler geometry and cryogenic treatment duration for enhanced tribological performance in advanced engineering applications.

Materials and Methods

Materials

Virgin *PTFE* powder (*Inoflon® 610*, *Gujarat Fluorochemicals Ltd.*, India) was used as the matrix material. According to the manufacturer, the nominal average particle size was ~200 μm, with a bulk density of 450 $g \cdot L^{-1}$, standard specific gravity of 2.15**,** and mould shrinkage of ~3.2%. Two mineral nano-fillers were employed: (i) nano-mica (layered silicate with flake-like morphology) and (ii) nano-alumina (Al_2O_3, equiaxed/globular morphology). Both were procured in powder form from *Platonic Nanotech Pvt. Ltd.* (*Jharkhand*, India) with a specified average particle size of ~50 nm. Based on our previous abrasive-wear study on *PTFE* nanocomposites [29], 1.0 wt.% nano-mica and 1.5 wt.% nano-alumina were selected as the optimal filler contents for the present study.

Prior to mixing, the *PTFE* and filler powders were pre-heated at 100°C for 2 h to remove moisture. The powders were then mixed using high-speed mechanical stirring followed by ultrasonic dispersion to ensure uniform distribution and minimize agglomeration.

Mechanical and tribological testing

Tensile tests were conducted on at least five specimens for each experimental condition, while compression and wear tests were performed with at least three replicates per condition. Average values and standard deviations were calculated for all measured properties. One-way *ANOVA* with *Tukey*'s post-hoc test ($p < 0.05$) was used to determine the statistical significance of observed differences. Error bars in graphical results represent the standard deviation.

Composite fabrication and sintering

Neat *PTFE*, *PTFE* + 1.0 wt.% nano-mica, and *PTFE* + 1.5 wt.% nano-alumina were fabricated by cold compression moulding at 13.8 MPa, followed by a sintering cycle. The specimens were prepared as cuboidal shapes of approximate dimensions 10 mm × 10 mm × 10 mm for compression, hardness, and wear testing, according to the respective *ASTM* standards.

Fig. 1 shows representative mechanical and tribological specimens of *PTFE* nanocomposites after cryo-treatment. The sample codes are as follows: ***PU*** is untreated neat *PTFE*; ***P8***, ***P12***, and ***P16*** indicate neat *PTFE* specimens cryo-treated by soaking at −185 °C for 8, 12, and 16 h, respectively; ***A8***, ***A12***, and ***A16*** denote nano-alumina-reinforced *PTFE* composites; and ***M8***, ***M12***, and ***M16*** represent nano-mica-reinforced *PTFE* composites subjected to the same cryogenic conditions.

Neat *PTFE*, *PTFE* + 1.0 wt.% nano-mica, and *PTFE* + 1.5 wt.% nano-alumina were fabricated by compression moulding, followed by a sintering cycle. Before moulding, the *PTFE* and filler powders were pre-heated at 100°C for 2 h to eliminate moisture. The mixed powders were then compressed individually at a pressure of 13.8 MPa. The green samples were then sintered according to the time-temperature cycle shown in Fig. 2. This process consolidated the *PTFE* powder and imparted strength to the final structure.

Fig. 1. Representative mechanical and tribological specimens of *PTFE* nanocomposites after cryogenic treatment

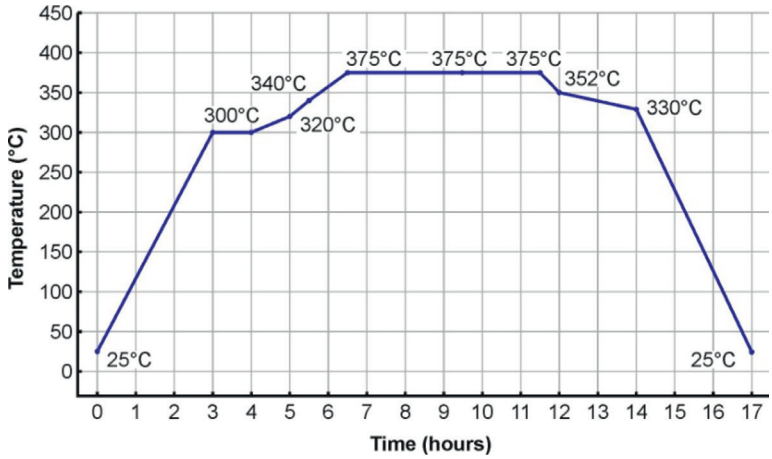

Fig. 2. Sintering cycle used for *PTFE* and its nanocomposites

Cryogenic treatment

Cryogenic treatment was performed on sintered neat *PTFE* and the optimized nanocomposites: *PTFE* + 1.0 wt.% nano-mica (flake-like filler) and *PTFE* + 1.5 wt.% nano-alumina (globular filler). Rectangular bars and plates machined from the sintered compacts were sealed in perforated polymer bags and placed in the vapour phase of liquid nitrogen within a custom-built liquid nitrogen-based cryo-chamber.

The cryo-cycle consisted of three steps:

1. Controlled cooling from room temperature to −185 ± 5 °C at 1.3–1.5 °C/min to minimize thermal shock;
2. Soaking at the target temperature for 8, 12, or 16 h;
3. Controlled warming to room temperature at 1.3–1.5 °C/min.

After the cycle, the specimens were conditioned at laboratory conditions for at least 24 h before testing. The soaking periods were selected based on previous studies on cryogenic treatment of *PTFE* and its composites [16, 26–28]. The treatment conditions are summarized in Table 1.

Table 1

Cryogenic treatment conditions

Sr. No.	Sample	Soaking time, h		
1	Neat *PTFE* (***PU***)	8 (***P8***)	12 (***P12***)	16 (***P16***)
2	*PTFE* + 1.0 wt.% nano-mica (***MU***)	8 (***M8***)	12 (***M12***)	16 (***M16***)
3	*PTFE* + 1.5 wt.% nano-alumina (***AU***)	8 (***A8***)	12 (***A12***)	16 (***A16***)

The samples were cryogenically treated in liquid nitrogen at −185 °C for 8, 12, and 16 h using a custom-built cryostat. The soaking periods were selected based on previous studies on cryogenic treatment of *PTFE* and its composites [16].

Mechanical testing

Tensile and compressive strength testing

Tensile strength and elongation at break were determined on a *Universal Testing Machine* (*UTM*, *International Equipment*, Mumbai) using dog-bone specimens (Type I) machined from sintered plates, in accordance with *ASTM D638*. The gauge section was cut parallel to the predominant pressing direction. Tests were conducted at room temperature with a constant cross-head speed of 50 mm/min. At least five specimens were tested for each material condition.

Compressive strength was determined on the same *Universal Testing Machine* by applying a gradually increasing load up to 50 % volumetric strain. The stress at this strain level was taken as the compressive strength. At least three specimens were tested per condition.

Abrasive wear testing and hardness

Abrasive wear performance was assessed using a pin-on-disc tribometer (*Magnum Engineering*, Bengaluru). Rectangular pin specimens (10 × 10 × 30 mm) were tested against 220-grade *SiC* abrasive paper fixed on a rotating steel disc under a normal load of 50 N. The track diameter was 80 mm, and the rotational speed was 200 rpm, corresponding to a linear sliding velocity of ~0.84 m/s. The test duration was 3 min at room temperature. Each specimen was cleaned, dried, and weighed to an accuracy of 0.1 mg before and after testing. The specific wear rate (*SWR*) was calculated from the mass loss, density, applied load, and sliding distance. At least three replicate tests were conducted for each condition.

Shore D hardness was measured using a durometer (*Veekay Instruments*) at five different locations on each specimen, and the average value was reported.

Statistical analysis

One-way *ANOVA*, followed by *Tukey*'s post-hoc test ($p < 0.05$), was used to determine the statistical significance of differences between groups. Average values and standard deviations were calculated for all properties. Error bars in figures represent standard deviation.

Structural and microstructural characterization

To elucidate the role of filler geometry and cryogenic treatment on the internal structure, the following techniques were employed on selected as-sintered and cryo-treated specimens.

Field emission gun scanning electron microscopy (FEG-SEM)

Tensile fracture and worn surfaces were examined using a *JEOL JSM-7610F* field emission scanning electron microscope. Surfaces were sputter-coated with a thin platinum layer using an auto-fine coater (*JEOL JEC-3000FC*). Micrographs were taken at various magnifications to analyze filler dispersion, matrix–filler interfacial quality, microcracking, particle pull-out, and wear mechanisms.

X-ray diffraction (XRD)

XRD patterns were recorded using a *Bruker D8 Advance* diffractometer with Cu *Kα* radiation ($\lambda \approx 1.5406$ Å) over a 2θ range of 10–100°, with a step size of 0.01° and a count time of 20 s per step. The degree of crystallinity and average crystallite size (calculated using *Scherrer's* equation) were determined with the *X'Pert High Score Plus* software after averaging three scans per sample [21].

Fourier transform infrared spectroscopy (FTIR)

FTIR spectra were recorded in the range 400–4000 cm^{-1} using a *Shimadzu FTIR-1-S Affinity* spectrometer equipped with an attenuated total reflectance (*ATR*) diamond probe. Each sample was scanned 45 times.

Characteristic bands of *PTFE*, nano-mica, and nano-alumina were analyzed to assess chemical integrity and possible interactions or degradation after cryogenic treatment.

Results and Discussion

Tensile and compressive strength testing

Fig. 3, *a* shows the tensile results for all untreated and cryo-treated samples. The tensile strength data clearly show that introducing fillers into *PTFE* enhances its mechanical performance, and that the effect depends strongly on filler morphology and cryogenic treatment duration. In the untreated condition, neat *PTFE* exhibits an average ultimate tensile strength of about 27.6 MPa. Adding 1 wt.% flake-like mica raises this to ~30.6 MPa, while adding 1.5 wt.% globular alumina yields ~29.8 MPa. Thus, even without cryogenic treatment, both fillers improve the reinforcement in *PTFE*, with mica providing the greatest initial increase in load-bearing capacity.

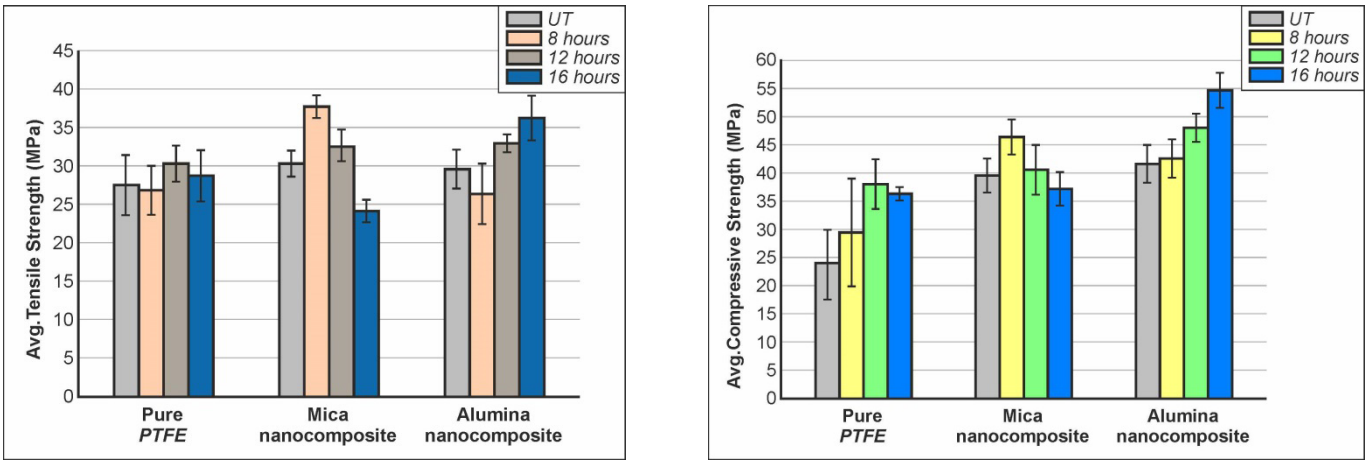

a *b*

Fig. 3. Variation in (*a*) tensile strength and (*b*) compressive strength of *PTFE*-based nanocomposites with cryogenic soaking time

Cryogenic treatment substantially modifies the mechanical response of the composites under investigation, with the geometry of the filler particles emerging as the decisive factor, based on the experimental evidence. Following an 8-h hold, unfilled *PTFE* exhibits little change, retaining a tensile strength of approximately 26.8 MPa. In contrast, the mica-filled system attains a peak value of about 37.9 MPa – roughly 25% above that of the untreated material – a gain that is plausibly associated with denser matrix packing and more effective stress transfer across the interfacial zones surrounding the platy particles. The alumina-filled composite behaves in the opposite manner, its tensile strength falling to about 26.6 MPa, i.e., returning to levels close to those of the pristine polymer.

Prolonging the treatment to 12 h tends to equalize the response. Strengths rise across all three systems: 30.3 MPa for unfilled *PTFE*, 32.8 MPa for the mica composite, and 33.0 MPa for the alumina composite.

At 16 h, the trends diverge markedly. The unfilled polymer registers a moderate decline to approximately 28.7 MPa, whereas the mica-filled composite undergoes a much more pronounced drop to about 24.2 MPa – below the as-received baseline. This deterioration is most likely attributable to microcracking and interfacial degradation along the extended planar surfaces of the mica platelets; during extended cooling, these interfaces act as preferential sites for stress concentration [21].

The nanosized alumina filler, conversely, continues to impart strengthening. At 16 h, the tensile strength reaches approximately 36.5 MPa – 23 % higher than the initial value and 27 % above that of the unfilled PTFE subjected to the identical treatment. The steady upward trend can reasonably be taken as indicative of a more isotropic stress distribution. The globular morphology, in contrast to the lamellar one, thus demonstrates superior resilience to prolonged cryogenic exposure.

Moreover, after 8 h of cryo-treatment, the response of all studied systems changes. Neat *PTFE* shows a slight reduction in ultimate tensile strength to ~26.8 MPa, indicating that short cryo-exposure alone does not produce a strengthening effect in the neat matrix. In contrast, the mica-nanocomposite peaks at ~37.9 MPa, a ~25% increase over its untreated strength, suggesting that limited cryo-cycling compacts the matrix around the flake-like platelets and improves interfacial stress transfer. The alumina–*PTFE* composite, however, decreases to ~26.6 MPa, similar to neat *PTFE* at 8 h, implying that at this stage the globular filler gains no structural advantage from cryo-processing.

At 12 h, all three systems reach a more favourable microstructural state. Neat *PTFE* increases to ~30.3 MPa (~10% above untreated), indicating improved crystallinity and defect healing [20]. The mica–*PTFE* composite decreases to ~32.8 MPa (~7% above untreated), while the alumina nanocomposite strengthens to ~33.0 MPa (~11% above untreated and ~9% higher than treated for 12 h neat *PTFE*).

A striking contrast appears at 16 h. Neat *PTFE* decreases slightly to ~28.7 MPa, still above the untreated baseline but below the 12 h optimum. The mica–*PTFE* composite drops sharply to ~24.2 MPa – ~36% lower than its 12 h peak and below its untreated value. This prolonged cryo-cycling probably induces microcracks and interfacial damage along the extended platelet–matrix interfaces, which act as stress concentrators [21]. Conversely, the nano-alumina-filled composite continues to improve, reaching ~36.5 MPa at 16 h (~23% above untreated and ~27% above 16 h-treated neat *PTFE*).

Thus, filler geometry controls not only the extent of reinforcement but also the optimum cryo-treatment window. Flake-like mica provides high reinforcement and the best absolute ultimate tensile strength at 8 h, but its performance is sensitive to over-exposure and deteriorates at 16 h. Conversely, globular alumina exhibits a monotonic increase in strength with treatment time, demonstrating greater resistance to microstructural damage from prolonged cryo-cycling.

The compressive strength results reveal a synergistic effect of cryo-treatment time and filler morphology on *PTFE*-based systems (Fig. 3,*b*). The compressive strength of neat *PTFE* (***PU***) is the lowest in the untreated state (~24 MPa) and increases to ~39.6 MPa and ~41.6 MPa with the addition of 1 wt.% flake-like mica (***MU***) and 1.5 wt.% globular alumina (***AU***), respectively, indicating that both fillers enhance the stiffness. Neat *PTFE* responds strongly to cryo-treatment: ***P8*** increases to ~29.7 MPa, ***P12*** peaks at ~38 MPa (~58% higher than ***PU***), and ***P16*** remains high at ~36.4 MPa, slightly below the 12 h optimum. This behavior is consistent with cryo-induced crystallinity enhancement, improved lamellar packing, and residual stress relief; excessively long soaking (16 h) may induce internal damage or stress, slightly reducing the strength.

For the mica-reinforced composite, the compressive strength increases from ~39.6 MPa (***MU***) to ~46.3 MPa at ***M8***, indicating that moderate cryo-treatment improves matrix crystallinity around the plate-like particles and enhances matrix–filler interfacial interaction. However, the strength decreases to ~40.8 MPa at ***M12*** and ~37.3 MPa at ***M16***, falling below the untreated value. This behavior suggests that in high-aspect-ratio systems with flake-like fillers, prolonged cryo-treatment promotes interfacial debonding, microvoid development along planar interfaces, and stress concentration under compressive loading, negating the initial benefits.

Conversely, the alumina-filled composite exhibits a nearly monotonic increase with cryo-soaking time: ~42.7 MPa at ***A8***, ~48.2 MPa at ***A12***, and ~54.5 MPa at ***A16*** – ~31% higher than the untreated ***AU*** (~41.6 MPa). The globular filler geometry likely ensures more isotropic stress transfer and allows the cryo-treated matrix to densify and lock around the particles without forming the extended weak planes characteristic of mica; therefore, longer soaking continuously improves compressive behavior rather than degrading it [21].

These trends are captured in the plotted figure for each system (***PU***re *PTFE*, the mica composite, and the alumina composite) across untreated, 8 h, 12 h, and 16 h treatments, respectively. The neat *PTFE* system exhibited maximum compressive strength at ***P12***, a rise-and-fall behavior with a maximum at ***M8*** for the mica system, and a steadily climbing sequence culminating in ***A16*** for the alumina system. The error bars indicate that the improvements observed at ***P12***, ***M8***, and especially ***A16*** are greater than the experimental scatter, confirming the consistency and reliability of the observed trends.

Overall, the compressive strength data reinforce the conclusion from tensile testing that filler morphology and cryo-treatment duration must be co-optimized: neat *PTFE* benefits strongly up to 12 h, mica-filled

PTFE has an optimum at shorter soaking (8 h) before interfacial degradation occurs, while alumina-filled *PTFE* continues to gain strength up to 16 h, making the 1.5 wt.% alumina composite at 16 h the best-performing material in compression among all studied samples.

Compressive strength is strongly influenced by both cryogenic treatment duration and filler morphology. Plate-like mica benefits from limited cryo-soaking (8 h), while nano-alumina-reinforced composites exhibit continuous strengthening up to 16 h. This finding directly complements the tensile analysis and reinforces the argument that filler morphology and cryogenic treatment schedule must be jointly optimized to control the performance of *PTFE*-based cryo-treated nanocomposites.

The elongation-at-break data (Fig. 4) show that cryogenic treatment progressively reduces ductility in all systems, but the extent of loss depends strongly on filler type and treatment duration. Neat *PTFE* has an average elongation of ~285% for the untreated sample (***PU***). This decreases to ~199% at 8 h (***P8***), ~184% at 12 h (***P12***), and ~142% at 16 h (***P16***), corresponding to ~30%, ~35%, and ~50% loss in ductility with increasing soaking time.

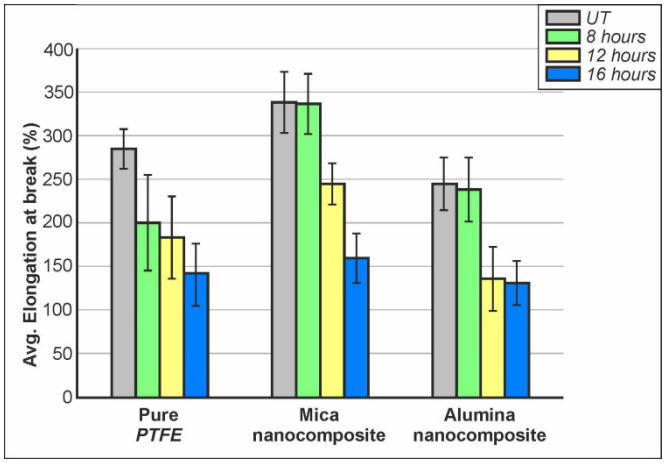

Fig. 4. Variation in elongation at break of *PTFE*-based nanocomposites with cryogenic soaking time

The mica–*PTFE* nanocomposite exhibits the highest initial elongation, with ***MU*** ~339%; the sample treated for 8 h (***M8*** ~337%) almost retains this value, indicating that short-duration cryogenic treatment does not significantly affect and may stabilize the strain-bearing microstructure in the flake-like filler system. However, beyond 8 h a sharp drop occurs: ***M12*** decreases to ~245% (~28% loss relative to ***MU***) and ***M16*** to ~157% (~54% loss), suggesting embrittlement due to excessive micro-cracking or constrained chain mobility at longer treatments.

The alumina nanocomposite, which starts at ***AU*** ~248% elongation, already has lower elongation than neat *PTFE*, consistent with globular alumina particles acting as stress concentrators. Nevertheless, the 8 h treatment (***A8*** ~242%) causes only a marginal reduction (~2–3%), indicating reasonable stability of the globular morphology at short times. With further cryo-treatment, elongation decreases steeply to ~138% for ***A12*** and ~131% for ***A16*** (~45–47% reduction from ***AU***), reflecting significant stiffening and embrittlement of the matrix.

Wear performance and hardness data analysis

The specific wear rate (*SWR*) of neat *PTFE* (***PU***) is the highest in the entire set, confirming its poor wear resistance compared with all composite and cryo-treated conditions. Filler addition, even without cryogenic treatment, reduces the *SWR*: the mica composite (***MU***) shows ~16% lower *SWR* than ***PU***, while the alumina composite (***AU***) gives an even larger reduction of ~22%. Thus, both fillers improve wear behavior over neat *PTFE*, with alumina being the more effective reinforcing phase in the untreated state. This is illustrated in Fig. 5, *a*, which shows that cryo-treatment reduces the *SWR* of both nanofilled *PTFE* systems compared to the untreated state, but the reduction is consistently stronger for the alumina-filled composite – most notably at the longest cryogenic exposure.

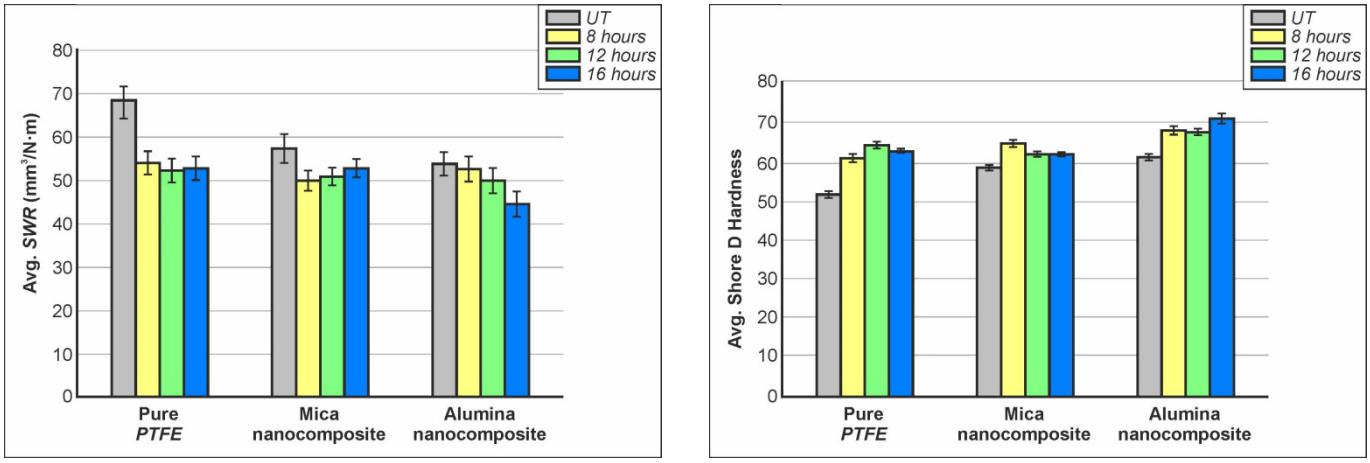

a *b*

Fig. 5. Effect of filler type and cryogenic treatment on specific wear rate (*a*) and hardness of *PTFE*-based nanocomposites (*b*)

Comparing the two fillers at equal cryo-treatment times (Fig. 5, *a*) further highlights their distinct efficiencies. At 8 h, ***M8*** (51.61) exhibits the lowest *SWR* among the three materials, slightly better than ***A8*** (54.32) and clearly better than ***P8*** (55.62), indicating that flake-like mica is highly effective in the early stages of cryogenic treatment, probably due to better load sharing along its high-aspect-ratio platelets. At 12 h, the ranking changes to ***A12*** (51.91) < ***M12*** (52.57) < ***P12*** (54.21), with alumina marginally outperforming mica, which is attributed to the fact that globular filler geometry contributes to lower *SWR* through improved load distribution and particle retention. At 16 h, alumina becomes clearly dominant as ***A16*** shows a markedly lower *SWR* (46.12) than both ***M16*** (54.10) and ***P16*** (54.41). Overall, alumina-filled *PTFE* responds more strongly and sustainably to prolonged cryo-treatment, ultimately giving the best wear resistance in the entire matrix–filler–treatment window.

The effect of cryo-treatment within each system shows different saturation behavior. For neat *PTFE*, cryo-treatment reduces *SWR* from 70.95 to ~55–54 (***P8–P16***), giving an improvement of ~22–24%; the optimum is ***P12*** (54.21), with only marginal change on further treatment (***P16***). For the mica composite, *SWR* decreases from 59.57 (***MU***) to 51.61 (***M8***), an additional ~13% improvement over ***MU*** and ~27% better than ***PU*** overall. However, extending the cryo-time beyond 8 h does not help; ***M12*** (52.57) and ***M16*** (54.10) show a slight loss of the benefit, suggesting that the microstructure and mica–matrix interface reach an optimum state early, after which excess treatment may introduce microcracks or stress concentrations.

In contrast, the alumina-filled composite exhibits a monotonic reduction in *SWR* with increasing cryogenic treatment duration. *SWR* decreases from 55.56 (***AU***) to 54.32 (***A8***), then to 51.91 (***A12***), and finally to 46.12 (***A16***). The 16 h treatment reduces *SWR* by ~17% compared to ***AU*** and by ~35% compared to ***PU***, indicating significant synergy between globular alumina particles and extended cryogenic treatment. Thus, alumina–*PTFE* acquires a more wear-resistant sliding surface after cryo-treatment compared to mica–*PTFE*, although both start from a similar baseline improvement over neat *PTFE*.

The morphopogy is significant. During cryogenic treatment, the *PTFE* matrix contracts around the fillers, improving mechanical interlocking. Globular alumina forms three-dimensional mechanical interlocking with more uniform radial compressive clamping of individual particles, resulting in greater particle retention and reduced debonding or pull-out. In contrast, flake-like mica has a large planar interface; differential contraction (*PTFE* vs mica) concentrates stress along platelet faces and edges, leading to a greater probability of microvoid formation, interfacial debonding, interfacial cracks, and delamination planes after prolonged cryo-soaking [24].

Regarding filler morphology, alumina morphology improves load transfer during sliding. Hard globular alumina particles act as uniformly distributed micro-load-bearing sites that reduce the effective contact of the soft *PTFE* matrix with the counterface and suppress excessive adhesive smearing. Mica platelets can

reinforce the matrix, but their geometry can create stress concentrations at platelet edges and promote shear along interlayer planes, encouraging microcrack initiation and flake-like detachment under repeated sliding stresses, especially after prolonged cryogenic treatment.

Finally, the performance of alumina is consistent with transfer-film and debris behavior during wear. If mica platelets debond, they tend to detach as flake-like debris that is more likely to plough or scratch the counterface, interrupting transfer-film continuity and limiting further *SWR* reduction at longer cryo-treatment durations. Alumina particles, being more equiaxed, are less likely to generate severe ploughing and more likely to promote the formation of a stable and compact *PTFE* transfer film; this stabilizes sliding and sustains the reduction in *SWR* with increased cryo-treatment duration, explaining alumina's superior wear response over mica in the cryo-treated condition.

Fig. 5,*b* depicts the effect of filler type and cryogenic treatment on the hardness of *PTFE*. For neat *PTFE* (***PU***), filler addition increases hardness substantially. The mica-filled composite (***MU***) is ~14.5% harder than ***PU***, while the alumina-filled composite (***AU***) is ~19.3% harder than ***PU***, indicating that alumina provides greater hardness than mica. Under cryo-treatment, alumina shows improvement in hardness compared to mica at each duration: at 8 h, ***A8*** is ~6.2% higher than ***M8***; at 12 h, ***A12*** is ~9% higher than ***M12***; and at 16 h, ***A16*** is ~15.6% higher than ***M16***. This confirms that the globular alumina phase delivers the highest and most stable hardness improvement across the cryo window compared to flake-like mica.

When these hardness trends are compared with the *SWR* data, a consistent inverse relationship emerges: conditions with higher hardness generally exhibit lower *SWR*. Relative to neat *PTFE*, ***P12*** shows a ~26.2% increase in hardness accompanied by a ~23.6% reduction in *SWR*; ***M8*** shows ~26.6% higher hardness with ~27.3% lower *SWR*; and the best condition, ***A16***, combines a ~39.1% hardness gain with ~35.0% lower *SWR* than ***PU***. Thus, cryo-treated alumina nanocomposites not only achieve the highest hardness but also deliver the largest percentage improvement in wear resistance, confirming that increased surface hardness resulting from optimized filler geometry and cryogenic treatment translates directly into superior tribological performance.

The results show that filler geometry and cryogenic treatment duration jointly govern the wear performance of *PTFE* nanocomposites, with nano-alumina exhibiting superior long-term tribological stability under prolonged cryogenic exposure.

XRD analysis

Fig. 6, *a* shows the *XRD* patterns of neat *PTFE* (***PU***), which exhibit a single *SEM*i-crystalline phase with the typical dominant reflection at $2\theta \approx 17.86–18.45°$, indexed to the (100) crystal plane, and a few additional reflections at higher angles of ~37.0–38.0° (110) and ~40.1–40.8° (200). The untreated sample (***PU***) has small peaks at 17.966° and 18.450°, which are usually attributed to heterogeneous crystalline populations and stresses introduced during processing; after cryogenic treatment, this region becomes much narrower with a single strong peak centered at ~18°, indicating increased uniformity of chain packing and stress relaxation [25].

The *XRD* patterns of cryo-treated *PTFE* (***P8***, ***P12***, and ***P16***) (Fig. 6, *a*) show the typical *SEM*i-crystalline *PTFE* profile, with a high-intensity reflection at $2\theta \approx 18°$, lower-intensity reflections at 31–32° , and a low-intensity or broadened crystalline contribution in the range 37–42°. Notably, no additional reflections or systematic peak shifts were observed following cryo-treatment, confirming that it did not produce any new crystalline phase or polymorphic transformation in *PTFE*. The main changes were in the form of peak intensity and broadening, indicating that cryogenic treatment had a significant effect on the degree of ordering, defect density, and crystallite size of the existing *PTFE* crystalline domains, but not on the phase identity. Among the cryo-treated neat *PTFE* samples, the diffraction pattern of ***P12*** exhibited a relatively stronger crystalline prominence compared with ***P16***.

The *XRD* profiles of both composite series (Fig. 6, *b*, *c*) retained the primary *PTFE* reflection at $2\theta \approx 18°$ and the secondary reflections at 31–32° and 37–42°, indicating that 1.0 wt.% nano-mica and 1.5 wt.% nano-alumina did not change the *PTFE* crystal structure. No individual high-intensity reflections that could be ascribed to mica or alumina were observed, suggesting that the filler incorporation mainly af-

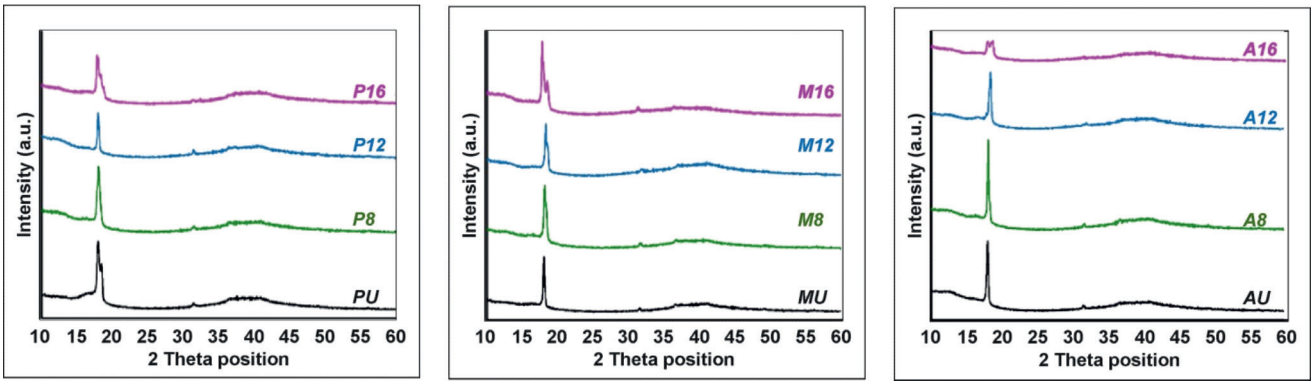

a *b* *c*

Fig. 6. *XRD* patterns of (*a*) neat *PTFE*, (*b*) the mica–*PTFE* composite, and (*c*) the alumina–*PTFE* composite in the untreated and cryo-treated states

fected the crystallization of *PTFE* without giving rise to a new phase as*SEM*blage. It is anticipated that the globular morphology of alumina should distribute stresses more isotropically than plate-like fillers and may partially restore *PTFE* ordering at longer cryo times.

Table 2 gives the crystallinity and average crystallite size data for all samples. Quantitatively, cryo-treatment produces a modest increase in crystallinity from 88.92% (***PU***) to 89.04% (***P8***), reaching a maximum of 90.15% (***P12***) before slightly decreasing to 89.64% (***P16***), demonstrating that 12 h provides the optimum crystallinity gain in neat *PTFE*. In parallel, the average crystallite size shows a pronounced refinement at intermediate cryo durations, decreasing from 172.0 nm (***PU***) to 114.6 nm (***P8***), with further reduction observed for ***P12***. These trends suggest that cryogenic exposure primarily promotes molecular re-ordering and stress-assisted rearrangement in *PTFE*, increasing the overall crystalline fraction while simultaneously altering crystallite coherence through defect generation/relaxation and reorganization with treatment time [26].

Table 2

Crystallinity and average crystallite size of the studied samples

Properties	PU	P8	P12	P16	MU	M8	M12	M16	AU	A8	A12	A16
Crystallinity (%)	88.92	89.04	90.15	89.64	88.17	89.66	84.58	82.86	86.95	82.16	85.95	88.21
Average crystallite size (nm)	172.0	114.6	100.61	163.66	189.5	162.5	252.5	329.0	157.0	238.75	163.2	128.0

For the mica composite, after cryo-treatment, crystallinity increases to a maximum of 89.66% at 8 h (***M8***), while the average crystallite size decreases to 162.5 nm, suggesting improved overall ordering through microstructural refinement. With further cryo-soaking, crystallinity drops sharply to 84.58% at 12 h (***M12***) and further to 82.86% at 16 h (***M16***), while the average crystallite size increases substantially. This trend of decreasing crystallinity with increasing crystallite size suggests that prolonged cryo-exposure in the presence of mica platelets promotes the growth and coalescence of crystalline domains, while simultaneously increasing interfacial microstrain and disorder around the *PTFE*–mica interfaces, thereby reducing the overall crystalline fraction.

For the alumina composite, after prolonged cryo-treatment, the system shows improved crystallinity and crystallite refinement: the crystallinity increases to 88.21% at 16 h, while the crystallite size decreases to a minimum of 128.0 nm compared to the untreated alumina composite (*AU*: 86.95% and 157.0 nm). This combination of rising crystallinity with decreasing crystallite size suggests that prolonged cryogenic exposure promotes reorganization and fragmentation of larger domains into finer, more uniformly ordered crystallites, improving the overall crystalline fraction despite the presence of filler–matrix interfaces.

From a mechanistic perspective, the improvement in tensile strength and the reduction in *SWR* are consistent with the *XRD* evidence of cryo-induced reordering in the *PTFE* crystalline phase and the stabilization of the load-transfer network around the fillers. Higher crystallinity increases the fraction of stiff, load-bearing domains in *PTFE*, which enhances hardness and tensile performance while simultaneously reducing the tendency for surface ploughing and adhesive pull-out during sliding, thereby reducing *SWR*. Meanwhile, crystallite size refinement generally promotes more homogeneous stress distribution, delays crack initiation, and improves microstructural stability under contact, as supported by the *UTS*, hardness, and wear resistance data. Thus, the optimum cryo durations – 12 h for neat *PTFE*, 8 h for the mica composite, and 16 h for the alumina composite – provide a coherent microstructure–property linkage that matches the observed mechanical and tribological data. Moreover, the *XRD* trends in crystallinity and crystallite size are consistent with the *SEM* micrographs; this correlation is discussed in detail in the following section.

The observed variations in crystallinity and crystallite size exceeded the experimental uncertainty, indicating meaningful structural evolution after cryogenic treatment.

FTIR analysis

FTIR response of neat PTFE to cryogenic treatment

The *FTIR* spectra of untreated and cryo-treated neat *PTFE* samples (8, 12, and 16 h) show that the main backbone vibrations remain essentially unchanged (Fig. 7). The *C–F* asymmetric and symmetric stretches at ~1,201–1,199 cm^{-1} and 1,145–1,143 cm^{-1}, the CF_2 wagging at 777–779 cm^{-1}, the CF_2 skeletal vibration at 634 cm^{-1}, and the *C–C* skeletal modes near 551 and 505–507 cm^{-1} are preserved across all soaking times.

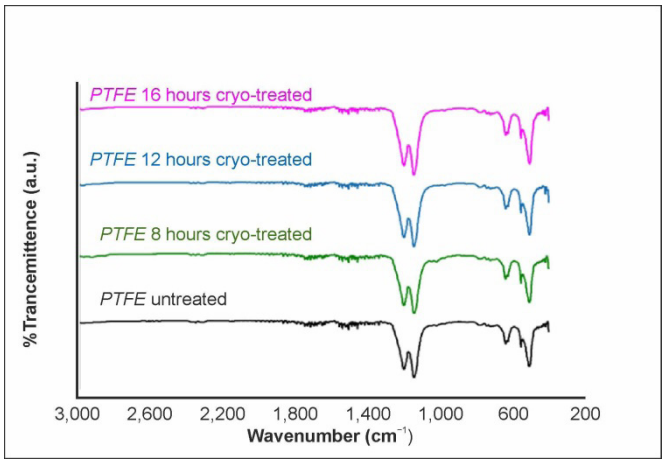

Fig. 7. Comparative *FTIR* spectra of untreated and cryo-treated *PTFE* (8, 12, and 16 h)

This invariance confirms that the crystalline *PTFE* backbone is structurally stable under cryogenic cycling and that any changes are restricted to surface or defect regions. In the high-wavenumber region, untreated *PTFE* exhibits *O–H* stretching bands at 3,786 and 3,701 cm^{-1}, associated with adsorbed surface moisture; these disappear after cryogenic treatment and are replaced by a single band at 3,741 cm^{-1} for all treated samples, indicating reorganisation of moisture into a more uniform, weakly hydrogen-bonded environment. A *C–H* stretch from weak organic residues at ~2,924 cm^{-1} shifts slightly to 2,926 cm^{-1} at 8 h and then vanishes at 12 and 16 h, while a new higher-wavenumber *C–H* band at 2,976 cm^{-1} appears at longer soak times, suggesting chain alignment. New bands at 1,867 and 1,739 cm^{-1} indicate the formation of small amounts of carbonyl groups, likely due to surface oxidation during controlled warming to room temperature or within defect-rich amorphous regions, and are accompanied by additional peaks at 1,514 and 1,454 cm^{-1} from unsaturated or oxygenated fragments [16, 26]. The *C–F* backbone peaks remain sharp and dominant, indicating that the carbonyl and unsaturated features can be viewed as low-level surface alterations without implying bulk degradation of the *PTFE* backbone. Overall, cryogenic treatment of neat *PTFE* affects primarily the surface chemistry without affecting the integrity of the crystalline backbone.

FTIR response of the nano-mica / 1 wt.% PTFE composite

The comparative *FTIR* spectra of untreated and cryo-treated mica composite are shown in Fig. 8. The *PTFE*/nano-mica composite exhibits a much stronger response to cryogenic treatment, with a richer and more persistent set of new *FTIR* features. The untreated material shows *OH* bands at 3,784 and 3,703 cm^{-1}, which change under cryogenic exposure: the higher band shifts to 3,898 cm^{-1} at 8 h and then disappears, while the lower band ~3,703 cm^{-1} becomes a stable band at 3,741 cm^{-1} at 8, 12, and 16 h. This evolution suggests considerable rearrangement of surface moisture and its interaction with silanol (*Si–OH*) groups on the mica surface, with subsequent stabilisation into a more homogeneous *O–H* environment.

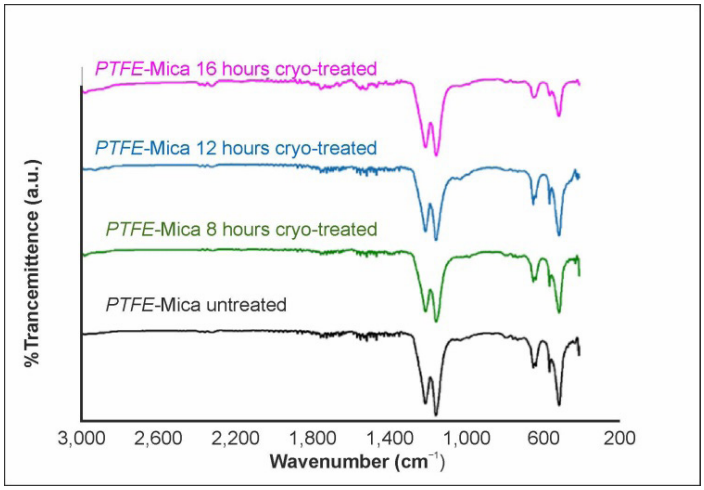

Fig. 8. Comparative *FTIR* spectra of untreated and cryo-treated mica–*PTFE* composite (8, 12, and 16 h)

The composite exhibits several carbonyl and defect-related bands in the mid-*IR* region, indicating greater chemical modification. New *C=O* bands appear at 1,969 cm^{-1} (only at 12 h), 1,867 cm^{-1} (12 and 16 h), 1,739–1,793 cm^{-1} (across all treated states), and 1,645–1,651 cm^{-1} (12 and 16 h). Unsaturated moieties at 1,514 cm^{-1} are observed at 12 and 16 h, while complex *C–H*/*C=C* bending at 1,454 cm^{-1} is present at all cryo times. Additional CF_3 bending or *C–F* deformation bands at 1,340 and 1,369 cm^{-1} at 12 and 16 h, respectively, indicate chain scission and the formation of CF_3-terminated or branched chain ends. A *Si–O* asymmetric stretch at ~1,020 cm^{-1} appears at 12 h, suggesting enhanced spectroscopic visibility of the surface nano-mica under specific cryo conditions, likely due to altered orientation or exposure of the platelets [16].

Although the main *C–F* backbone peaks near 1,192–1,199 and 1,143–1,145 cm^{-1} remain, the CF_2 wagging band at 779 cm^{-1}, present at 8 and 12 h, disappears at 16 h, indicating a loss of regular CF_2 conformations at long soaking times due to stress concentration a t the lamellar interfaces. CF_2 skeletal vibrations shift from 632 to 634–637 cm^{-1}, and a new *C–C* skeletal band at 561 cm^{-1} appears in all treated states, indicating significant repacking and increased heterogeneity of the *PTFE* backbone around the rigid flake-like fillers.

FTIR response of the PTFE / 1.5 wt.% nano-alumina composite

In the *PTFE*/nano-alumina composite, cryogenic treatment produces moderate but distinctive changes in the hydroxyl and interfacial regions. Fig. 9 shows the comparative *FTIR* spectra of untreated and cryo-treated *PTFE*–alumina composites. The untreated composite shows no prominent high-wavenumber *O–H* band, whereas all cryo-treated specimens display new features at 3,739–3,741 cm^{-1}, assigned to surface moisture and hydroxylated alumina sites that become more IR-active after cryo-cycling. Their persistence over time suggests a stable alumina–moisture/*PTFE* interfacial environment. A *C–H* signal at ~2,976–2,974 cm^{-1} is present at all soaking times but is absent in the untreated form, likely due to trace organic residues or chain-end/defect sites exposed at the filler–matrix interface. Bands associated with carbonyls and defects are relatively weak and short-lived: *C=O* at 1739 cm^{-1} appears at 8 and 12 h and disappears at 16 h, while

bands at 1,546; 1,514, and 1,454 cm^{-1} appear intermittently, indicating initial oxidative fragments that subsequently relax, reorient, or recombine.

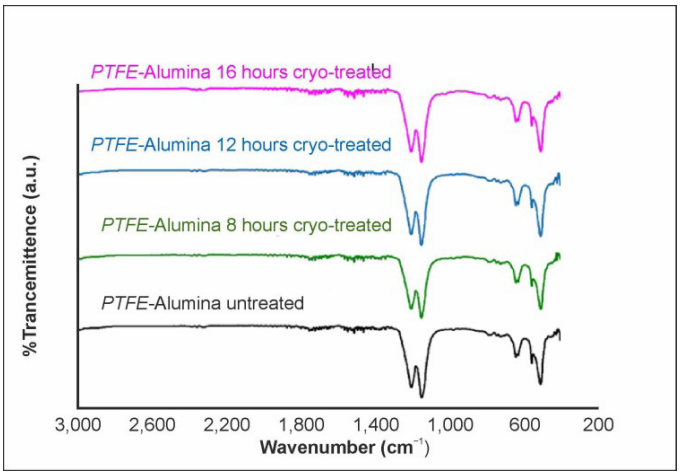

Fig. 9. Comparative *FTIR* spectra of untreated and cryo-treated alumina–*PTFE* composite (8, 12, and 16 h)

Notably, the *C–F* asymmetric and symmetric stretches remain at 1,199 and 1,145 cm^{-1}, respectively, indicating that the *PTFE* backbone is intact. The CF_2 wagging band at 779–777 cm^{-1}, which is absent in the untreated composite, appears as a new, sharp feature in all cryo-treated specimens, suggesting increased ordering or constrained conformations of CF_2 units in the vicinity of the alumina particles; a secondary wagging mode at 719 cm^{-1} is observed only at 12 h and is considered to represent an intermediate ordering state. The CF_2 skeletal and *C–C* skeletal bands do not disappear, with only small changes in chain packing around the globular nanoparticles, in contrast to the significant disruption observed in other systems [27]. Thus, the nano-alumina composite exhibits stable *O–H* signatures, weak and temporary oxidation, and enhanced CF_2 ordering, all of which indicate a well-organized interfacial region.

Effects of filler morphology as unveiled by FTIR

Overall, the *FTIR* data reveal how filler geometry controls the cryogenic behavior of *PTFE* composites. The addition of globular nano-alumina (1.5 wt.%) introduces point contacts of the *PTFE* matrix with isotropic particles. Spectroscopically, this is reflected in long-lasting *O–H* bands attributed to alumina surfaces, short-lived and weak carbonyl or unsaturated bands, and stable, sharp CF_2 backbone and wagging bands. These observations indicate that the globular geometry experiences more uniform stress without local stress concentrations and allows a relatively ordered *PTFE* environment around the particles. Cryo-induced defects remain mild, and the interfacial region is chemically and structurally stable, consistent with the enhanced mechanical properties observed in tensile and hardness tests.

In contrast, flake-like nano-mica (1 wt.%) consists of high aspect-ratio platelets with extended planar interfaces and sharp edges. The *FTIR* spectra exhibit strong and persistent carbonyl bands across a wide wavenumber range, unsaturated and defect bands at 1,514 and 1,454 cm^{-1}, new CF_3 deformation bands at 1,340 and 1,369 cm^{-1}, irregular C–H and CO_2 spectral features, activation of *Si–O* stretching, disappearance of the CF_2 wagging mode at long soaking times, and emergence of a new *C–C* skeletal band at 561 cm^{-1}. These features are characteristic of more severe interfacial stress, *PTFE* chain scission, defluorination, and structural heterogeneity driven by the platelet geometry of mica, and correlate with the comparatively poorer tensile performance of the mica-filled composite.

SEM analysis

Fig. 10 shows comparative *SEM* micrographs of untreated and cryo-treated neat *PTFE* (8, 12, and 16 h). The micrographs show that untreated *PTFE* (***PU***) exhibits a comparatively compact, smoother fracture morphology dominated by lamellar/plate-like features with limited fibrillation, suggesting lower

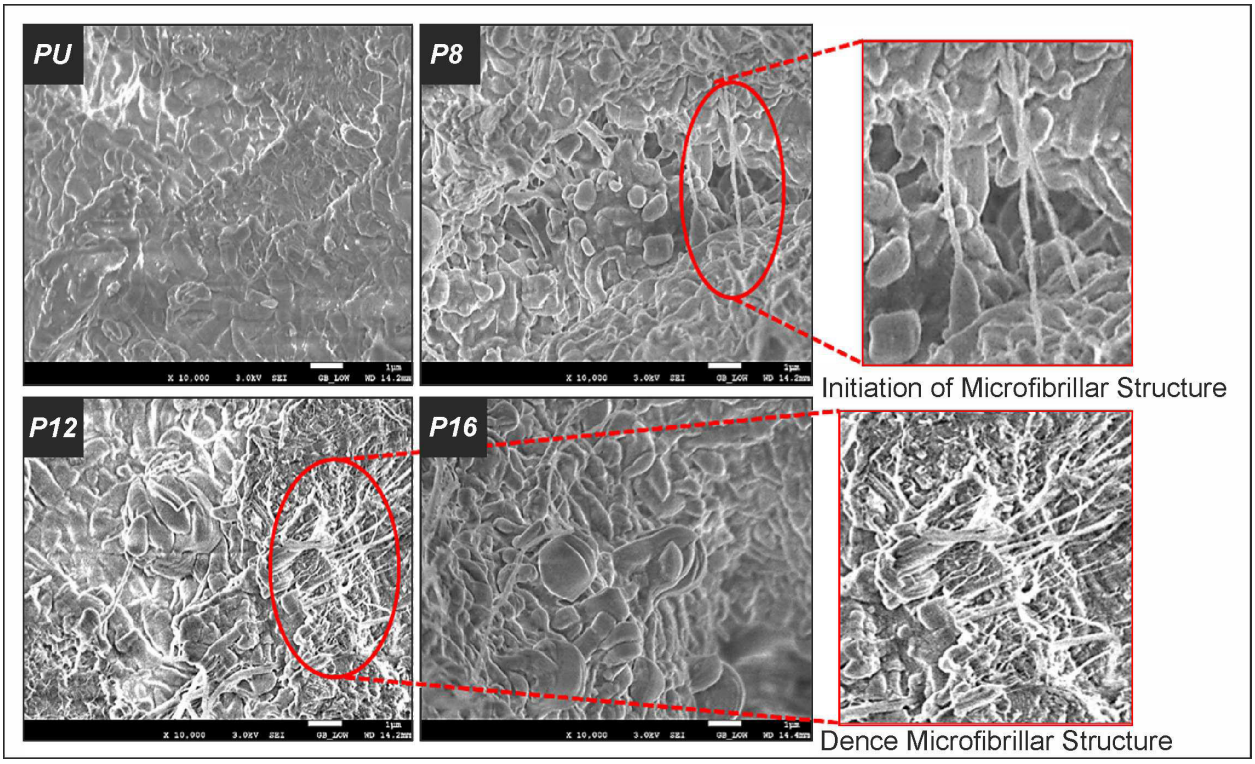

Fig. 10. Comparative *SEM* images of untreated and cryo-treated neat *PTFE* (8, 12, and 16 h

microscale crack-bridging and reduced internal mechanical interlocking. After cryogenic soaking, the surface transforms progressively: ***P8*** (8 h) displays increased roughness and the onset of fibril-like strands bridging local depressions, indicating initiation of fibrillation and microstructural rearrangement consistent with the known ability of *PTFE* to develop fibrillar structures under suitable thermomechanical conditions. The most prominent change occurs in ***P12*** (12 h), where a dense microfibrillar network spans across the fractured surface.

The mechanical significance of this fibrillar network is that fibrils can bridge the crack plane, deflect crack propagation, and facilitate energy dissipation through stable fibril formation/pull-out – a well-known toughening mechanism in *PTFE* fracture studies. While 'node–fibril' type microstructures are commonly reported in the literature and are directly related to load sharing and mechanical response, *SEM* observations of fibrils and nodes are commonly used to interpret tensile property changes. By comparison, ***P16*** (16 h) already exhibits fibrillar features but with a more disturbed and overdeveloped, partially disrupted morphology (bundling, tearing, and disrupted zones), which may involve micro-voiding or stress concentrators that compromise the effectiveness of a continuous bridging network [28].

Thus, the *SEM* data suggest that the optimum condition is observed at 12 h of cryogenic treatment: this is the best condition for generating the longest and most continuous microfibrillar structure, providing the greatest crack-bridging and load-transfer paths, which is consistent with the finding that tensile and compressive strengths are maximized at 12 h. This optimum soak-time behavior is also consistent with the general concept that cryogenic treatment can alter polymer microstructure (e.g. through rearrangement, thermal-stress effects, and changes in crystallinity or phase organization), and that the property response is a time-dependent function (not monotonic). Notably, the literature on cryogenic treatment of *PTFE* has also suggested an optimum at ~12 h (usually just below –185 °C) with the enhancement attributed to structural and crystallinity effects, which supports the use of 12 h as the most effective treatment duration for strengthening in the present study.

Fig. 11 shows comparative *SEM* micrographs of untreated and cryo-treated mica–*PTFE* nanocomposites. The micrographs of the untreated mica composite (***MU***) reveal a relatively homogeneous, compact fracture morphology with mainly matrix-dominated tearing/cleavage features and no significant platelet signatures at the surface, indicating limited crack-bridging by the reinforcement and less efficient stress transfer between *PTFE* and the mica phase.

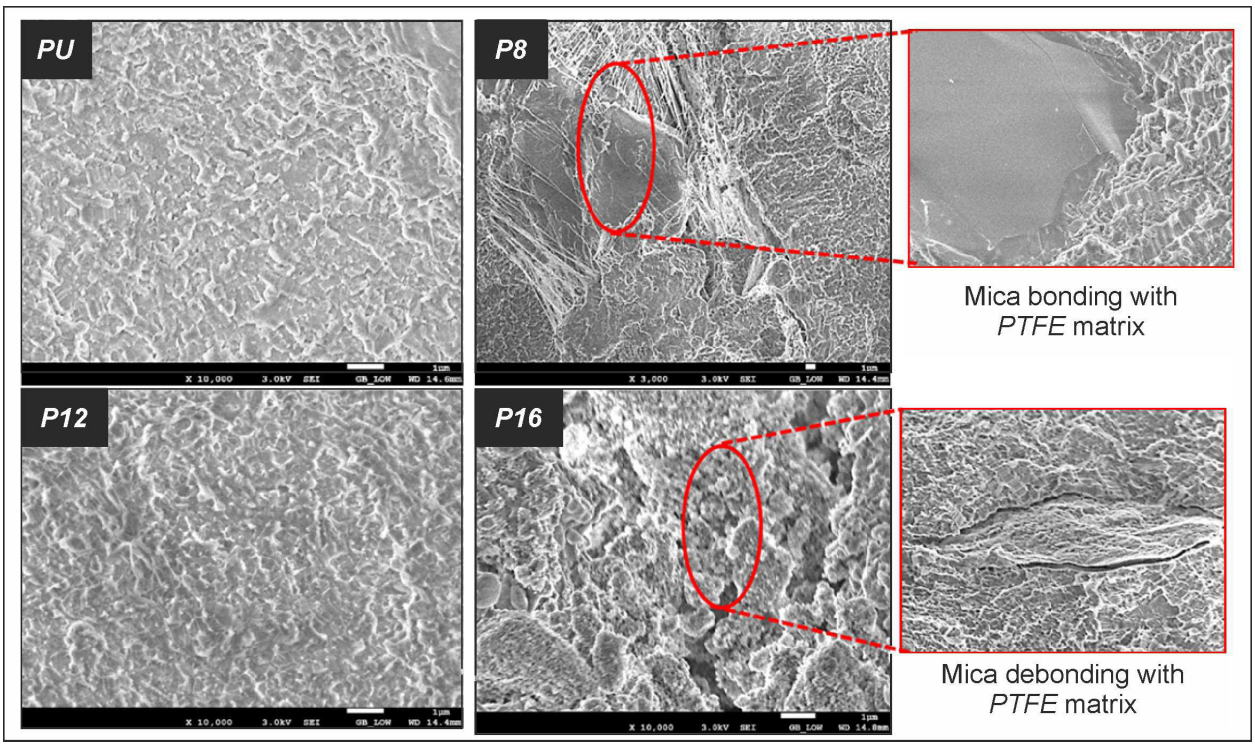

Fig. 11. Comparative *SEM* images of untreated and cryo-treated mica–*PTFE* nanocomposites (8, 12, and 16 h)

After cryogenic soaking, the microstructure becomes more differentiated and more diagnostic of the filler–matrix interface quality. At ***M8*** (8 h), a large mica platelet is visible as a smooth, planar area and, more importantly, the surrounding *PTFE* intimately conforms to the platelet boundary without visible gaps; fine drawn features around the platelet indicate mechanical interlocking and a good interface.

The interface state (adhesion/anchoring vs. debonding) is a primary factor controlling composite performance: good adhesion improves load transfer, while weak adhesion promotes interfacial separation and premature failure [30]. In platelet-reinforced systems, strong interface quality also promotes crack deflection and crack pinning around the platelet (higher energy absorption), whereas weak bonding tends to cause debonding, microvoiding, and platelet pull-out, which reduces strength – mechanisms widely used to interpret fracture surfaces in platelet-filled polymer composites. At ***M12*** (12 h), the fracture surface appears more homogenized and heavily deformed, but with less clear evidence of the "tight" platelet–matrix interface observed at ***M8***, implying reduced effectiveness of the interface-driven reinforcement [30]. Finally, ***M16*** (16 h) shows the most adverse morphology, with a pronounced delamination-like crack in the magnified region — consistent with interfacial debonding and microcrack growth. Such damage is plausible under prolonged cryogenic exposure because polymers and composites become more brittle and susceptible to thermal-stress-driven microcrack initiation and delamination as stresses accumulate.

Thus, the *SEM* evidence supports 8 h cryo-treatment as the optimum condition for the mica composite: it produces the best apparent mica–*PTFE* bonding and interfacial continuity, enabling more efficient load transfer and crack-path disruption, which directly explains the peak tensile and compressive strengths at 8 h in agreement with the mechanical test data.

Fig. 12 shows comparative *SEM* micrographs of untreated and cryo-treated alumina–*PTFE* nanocomposites. The untreated alumina composite (***AU***) exhibits a matrix-dominated fracture morphology with a relatively coarser, less fibrillated surface; the large globular alumina particle appears surrounded by regions suggesting interfacial discontinuity or incipient separation, implying that load transfer from *PTFE* to the ceramic phase is not fully realized in the untreated state.

After cryogenic soaking, the fracture morphology develops gradually. ***A8*** (8 h) shows enhanced surface roughness and localized deformation, but the magnified area reveals interfacial disturbances around alumina-rich regions (early-stage debonding or particle pull-out imprints), indicating that the reinforcement

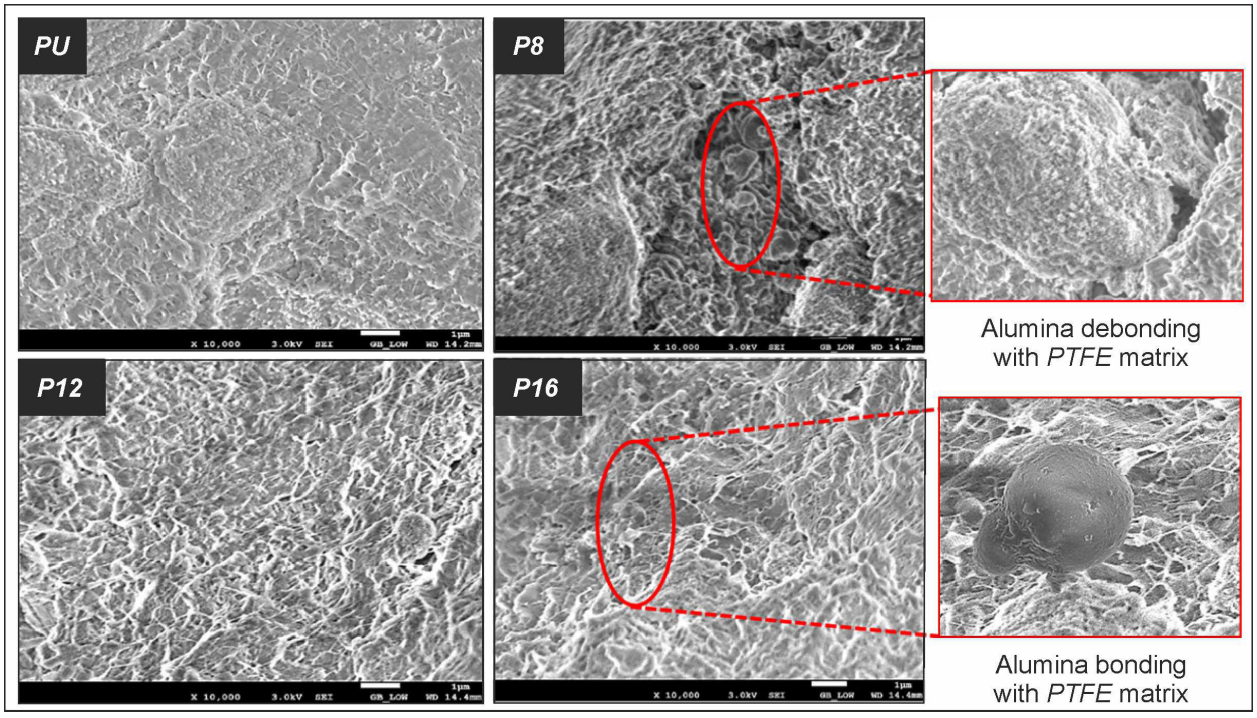

Fig. 12. Comparative *SEM* images of untreated and cryo-treated alumina–*PTFE* nanocomposites (8, 12, and 16 h)

was not yet uniformly stabilized in the matrix. ***A12*** (12 h) exhibits more drawn *PTFE* features across the surface, indicating increased plastic deformation, but the reinforcement is not as clearly locked-in as at the longest soaking time. The most pronounced modification occurs at ***A16*** (16 h), where the magnified area displays a globular alumina particle well-positioned within a fibrillated *PTFE* network, with the matrix tightly anchored around the particle rather than separating from it. This morphology enhances mechanical interlocking of *PTFE* fibrils by the filler and suppresses simple particle pull-out, promoting stress transfer and energy dissipation during fracture.

The literature indicates that the efficiency of stress transfer between ceramic particles and the *PTFE* matrix is determined by the strength of interfacial bonding: stronger interfaces allow the filler to participate more effectively in load sharing rather than acting as debonding defects [30]. Here, the *SEM* evidence suggests that 16 h is the optimal treatment for the alumina composite: the most prominent microstructural feature is enhanced alumina–*PTFE* interfacial continuity and anchoring, which likely underlies the peak tensile and compressive strengths, in agreement with the mechanical test results.

FTIR results indicate that the surface and defect chemistry of pure *PTFE*, including moisture, CO_2 and any minor oxidative species, are largely affected by the cryogenic treatment, whereas the crystalline C-F backbone structure is not affected. Adding globular nano-alumina results in a composite whereby cryo-cycling causes only a small and temporary oxidative signal and in fact improves local CF_2 arrangement about the particles, a stable interfacial stress state. Conversely, the addition of high aspect-ratio nano-mica leads to large-scale, long-lasting oxidative and defect-related structures, backbone distortion and enhanced chemical heterogeneity at cryogenic temperature, indicative of strong interfacial stress and chain scission. In this way, the *FTIR* data can directly contribute to the conclusion that filler geometry; spherical and flaky filler geometries control the influence of the cryo-treatment on the interfacial chemistry and backbone integrity of *PTFE* composites, and it is this microscopic behavior that leads to the differences in macroscopic mechanical behavior.

Overall, the *XRD*, *FTIR*, and *SEM* data collectively demonstrate that filler geometry strongly governs the structural evolution, interfacial stability, and microstructural response of *PTFE* nanocomposites under prolonged cryogenic treatment.

The results show a geometry-dependent response of *PTFE* nanocomposites to cryogenic treatment. Neat *PTFE* shows optimal performance at 12 h. The nano-mica (flake-like) composite performs best at 8 h

but deteriorates with longer treatment due to interfacial debonding and microcrack formation along planar interfaces. In contrast, the nano-alumina (globular) composite exhibits progressive improvement, achieving superior tensile strength, compressive strength, hardness, and wear resistance at 16 h. This is attributed to better isotropic stress distribution, stronger particle anchoring, and more stable filler–matrix interfaces, as supported by *XRD* (crystallinity refinement), *FTIR* (stable interfacial chemistry), and *SEM* (improved mechanical interlocking).

Thus, filler geometry controls not only the extent of reinforcement but also determines the optimal cryogenic treatment duration. Globular nano-alumina is preferable for prolonged cryogenic treatment, while flake-like nano-mica is suitable only for shorter durations. These findings provide a basis for designing high-performance cryo-treated *PTFE* nanocomposites for advanced tribological applications such as seals, bearings, and piston rings.

Conclusion

Cryogenic treatment at –185 °C modifies the properties of *PTFE* and its nanocomposites in a time- and filler-geometry-dependent manner. The main findings are as follows:

1. Neat *PTFE* achieves the best overall balance of mechanical and tribological properties after 12 h of cryogenic treatment owing to microstructural re-ordering and increased crystallinity.

2. The flake-like nano-mica composite exhibits its optimum performance at an 8 h soaking time. Prolonged cryogenic treatment (beyond 8 h) leads to interfacial debonding, microcracking, and deterioration of mechanical and wear properties due to its high-aspect-ratio planar interfaces.

3. The globular nano-alumina composite shows progressive improvement with soaking time and delivers the best combination of tensile strength, compressive strength, hardness, and wear resistance at 16 h, owing to stable interfacial anchoring and isotropic stress distribution.

4. Filler geometry strongly influences the effectiveness of cryogenic treatment. Globular nano-alumina is more suitable for prolonged cryogenic treatment, while flake-like nano-mica performs better under shorter treatment durations.

5. The mechanical, tribological, and microstructural results (*XRD*, *FTIR*, and *SEM*) are mutually consistent and confirm ***P12*** (neat *PTFE*), ***M8*** (nano-mica), and ***A16*** (nano-alumina) as the optimum conditions.

This study provides a basis for understanding structure–property relationships and shows that filler morphology and cryogenic treatment duration must be co-optimized to achieve enhanced performance in *PTFE* nanocomposites for advanced tribological applications such as seals, bearings, and piston rings.

References

1. Deshwal D., Belgamwar S.U., Bekinal S.I., Doddamani M. Role of reinforcement on the tribological properties of polytetrafluoroethylene composites: A comprehensive review. *Polymer Composites*, 2024, vol. 45, pp. 14475–14497.

2. Puts G.J., Crouse P., Ameduri B.M. Polytetrafluoroethylene: Synthesis and characterization of the original extreme polymer. *Chemical Reviews*, 2019, vol. 119, pp. 1763–1805.

3. Dhanumalayan E., Joshi G.M. Performance properties and applications of polytetrafluoroethylene (PTFE) – A review. *Advanced Composites and Hybrid Materials*, 2018, vol. 1, pp. 247–268.

4. Zhao G., Zhu S. Al_2O_3/PTFE composites for marine self-lubricating bearings: Modulation mechanism of alumina particle size on material mechanical properties and tribological behaviour. *Lubricants*, 2025, vol. 13 (9). DOI: 10.3390/lubricants13090377.

5. Kinloch A.J., Taylor A.C. The mechanical properties and fracture behaviour of epoxy–inorganic micro- and nano-composites. *Journal of Materials Science*, 2006, vol. 41, pp. 3271–3297.

6. Ongaro G., Pontefisso A., Zeni E., Lanero F., Famengo A., Zorzi F., Zaccariotto M., Galvanetto U., Fiorentin P., Gobbo R., Bertani R., Sgarbossa P. Chemical and mechanical characterization of unprecedented transparent epoxy–nanomica composites – New model insights for mechanical properties. *Polymers*, 2023, vol. 15, p. 1456. DOI: 10.3390/polym15061456.

7. Cheng H.Y., Jiang G.J., Hung J.Y. Enhanced mechanical and thermal properties of PS/mica and PMMA/mica nanocomposites by emulsion polymerization. *Polymer Composites*, 2009, vol. 30 (4), pp. 351–356.

8. Ziadeh M., Fischer B., Schmid J., Altstädt V., Breu J. On the importance of specific interface area in clay nanocomposites of PMMA filled with synthetic nano-mica. *Polymer*, 2014, vol. 55 (16), pp. 3770–3781. DOI: 10.1016/j.polymer.2014.05.063.

9. Panda J.N., Bijwe J., Pandey R.K. On the significant enhancement in the performance properties of PAEK composite by inclusion of a small amount of nano-mica particles. *Tribology International*, 2019, vol. 136, pp. 87–104.

10. Lapčík L., Maňas D., Lapčíková B., Vašina M., Staněk M., Čépe K., Vlček J., Waters K.E., Greenwood R.W., Rowson N.A. Effect of filler particle shape on plastic–elastic mechanical behavior of high density poly(ethylene)/mica and poly(ethylene)/wollastonite composites. *Composites Part B: Engineering*, 2018, vol. 141, pp. 92–99. DOI: 10.1016/j.compositesb.2017.12.035.

11. McElwain S.E., Blanchet T.A., Schadler L.S., Sawyer W.G. Effect of particle size on the wear resistance of alumina-filled PTFE micro- and nanocomposites. *Tribology Transactions*, 2008, vol. 51 (2), pp. 247–253.

12. Tian Y., Li R., Wang Z., Zheng S., Che Q., Zhang J. Hybrid of micro-aramid and nano-alumina prominently enhanced the wear resistance of polytetrafluoroethylene composites. *Journal of Reinforced Plastics and Composites*, 2024, vol. 44, pp. 2138–2148. DOI: 10.1177/07316844241253467.

13. Tóth L.F., De Baets P., Szebényi G. Thermal, viscoelastic, mechanical and wear behaviour of nanoparticle filled polytetrafluoroethylene: A comparison. *Polymers*, 2020, vol. 12 (10), p. 1940.

14. Burris D.L., Sawyer W.G. Improved wear resistance in alumina-PTFE nanocomposites with irregular shaped nanoparticles. *Wear*, 2006, vol. 260, pp. 915–918.

15. Burris D.L., Sawyer W.G. Tribological sensitivity of PTFE/alumina nanocomposites to a range of traditional surface finishes. *Tribology Transactions*, 2005, vol. 48 (2), pp. 147–153.

16. Damdhar V.S., Pande K.N., Peshwe D.R., Gogte C.L. To investigate the wear mechanism on cryogenic treatment of PTFE-mica filled composite coatings in cookware. *Transactions of the Indian Institute of Metals*, 2015, vol. 68 (4), pp. 611–621. DOI: 10.1007/s12666-014-0491-7.

17. Brown E.N., Dattelbaum D.M. The role of crystalline phase on fracture and microstructure evolution of polytetrafluoroethylene (PTFE). *Polymer*, 2005, vol. 46 (9), pp. 3056–3068.

18. Vasilev A.P., Struchkova T.S., Nikiforov L.A., Okhlopkova A.A., Grakovich P.N., Shim E.L., Cho J.-H. Mechanical and tribological properties of polytetrafluoroethylene composites with carbon fiber and layered silicate fillers. *Molecules*, 2019, vol. 24 (2), p. 224.

19. Lebedev Yu.A., Korolev Yu.M., Polikarpov V.M., Ignat'eva L.N., Antipov E.M. X-ray powder diffraction study of polytetrafluoroethylene. *Crystallography Reports*, 2010, vol. 55 (4), pp. 609–614.

20. Smolyanskii A.S., Politova E.D., Koshkina O.A., Arsentyev M.A., Kusch P.P., Moskvitin L.V., Slesarenko S.V., Kiryukhin D.P., Trakhtenberg L.I. Structure of polytetrafluoroethylene modified by the combined action of γ-radiation and high temperatures. *Polymers*, 2021, vol. 13 (21), p. 3678.

21. Patterson A.L. The Scherrer formula for X-ray particle size determination. *Physical Review*, 1939, vol. 56, pp. 978–982.

22. Brown E.N., Rae P.J., Bruce Orler E., Gray G.T., III, Dattelbaum D.M. The effect of crystallinity on the fracture of polytetrafluoroethylene (PTFE). *Materials Science and Engineering: C*, 2006, vol. 26 (8), pp. 1338–1343.

23. Piwowarczyk J., Jędrzejewski R., Moszyński D., Kwiatkowski K., Niemczyk A., Baranowska J. XPS and FTIR studies of polytetrafluoroethylene thin films obtained by physical methods. *Polymers*, 2019, vol. 11 (10), p. 1629.

24. Yang D., Niu Q., Wang H., Gao G., Zhao G., Yang H., Lv T., Yang S., Zhang J. Enhancement of friction and wear performance of polytetrafluoroethylene composites through the synergistic effect of hard fillers. *Polymer Composites*, 2024, vol. 46, pp. 4112–4128. DOI: 10.1002/pc.29227.

25. Lv W., Wang T., Wang Q., Yap K.K., Song F., Wang C. Tribological and mechanochemical properties of nanoparticle-filled polytetrafluoroethylene composites under different loads. *Polymers*, 2024, vol. 16 (7). DOI: 10.3390/polym16070894.

26. Cui Y., Yan J., Li J., Chen D., Wang Z., Yin W., Wu Z. Cryogenic mechanical properties and stability of polymer films for liquid oxygen hoses. *Polymers*, 2023, vol. 15 (16), p. 3423. DOI: 10.3390/polym15163423.

27. Nikonovich M., Ramalho A., Emami N. Effect of cryogenic aging and test-environment on the tribological and mechanical properties of PEEK composites. *Tribology International*, 2024, vol. 194. DOI: 10.1016/j.triboint.2024.109554.

28. Kapitonova I., Tarasova P., Lazareva N., Okhlopkova A., Danilova S. Mechanical and tribological properties of polymer composite materials based on PTFE filled with natural mica and magnesium aluminium oxide. *Tribology and Materials*, 2025, vol. 4 (2), pp. 56–65. DOI: 10.46793/tribomat.2025.010.

29. Dong Z., Tang H., Yang B., Wang S., Li Y., Liu L. Molecular dynamics simulation and experimental study of the mechanical and tribological properties of GNS-COOH/PEEK/PTFE composites. *Polymers*, 2024, vol. 16. DOI: 10.3390/polym16182572.

30. Huang S., Yin Y., Fang X., Wei D., Yuan Y., Chen Q. The dominant role of nanofiller-induced tribochemistry in determining the tribological characteristics of PTFE composite systems. *Polymer Composites*, 2025, vol. 47, pp. 4480–4489. DOI: 10.1002/pc.70440.

Conflicts of Interest

The authors declare no conflict of interest.